Density Functional Theory in Surface Science and Heterogeneous Catalysis

J.K. Nørskov, M. Scheffler, and H. Toulhoat

Abstract

Solid surfaces are used extensively as catalysts throughout the chemical industry, in the energy sector, and in environmental protection. Recently, density functional theory has started providing new insight into the atomic-scale mechanisms of heterogeneous catalysis, helping to interpret the large amount of experimental data gathered during the last decades. This article shows how density functional theory can be used to describe the state of the surface during reactions and the rate of catalytic reactions. It will also show how we are beginning to understand the variation in catalytic activity from one transition metal to the next. Finally, the prospects of using calculations to guide the development of new catalysts in industry will be discussed.

Keywords: *catalytic, simulation, surface reaction.*

Introduction

A catalyst is a substance that can facilitate a chemical reaction; catalytic technology provides a range of products, from fuels and fertilizers to plastics and pharmaceuticals. Catalysis is also used to clean emissions from cars, power plants, and industrial production. The importance of catalysis to society is reflected by estimates suggesting that more than 20% of manufacturing in the industrialized world is dependent on catalysis.[1] Most catalysts used in industry are solids, and the catalysis typically takes place on the surface of nanoparticles of the active material. We are rapidly approaching the 100th anniversary of the first large-scale industrial catalytic process, ammonia synthesis, introduced by Haber and Bosch.[2] Since then, the understanding of the way solid surfaces can interact with gas-phase molecules, break them down, and form new products has increased enormously, and recently, catalyst development has been refined substantially by the introduction of parallel synthesis and screening methods.[3]

There are new developments which show that progress is being made toward a new, molecular-scale picture of the way solids work as catalysts. One very important development is that electronic-structure calculations based primarily on density functional theory (DFT) are beginning to provide information that is hard to obtain by experimental methods. The calculations can illuminate the nature of the transition states of molecules undergoing chemical transformation at the surface of a solid. In doing so, trends in reactivity and conceptual models of the way solids act as catalysts can be developed.

In this article, we will briefly review some of the developments that have made it possible to understand how surface-catalyzed reactions proceed. First, we will discuss how DFT calculations can be used to describe the working state of a catalyst under realistic high-pressure and high-temperature operation. Next, we will discuss how an understanding of the variations in catalytic activity from one material to the next is beginning to emerge, and, finally, we will show how progress in the theoretical description of surface reactions has an impact on catalyst development in industry.

Thermodynamic and Kinetic Modeling: General Concepts

This section discusses how atoms or molecules from an environment—for example, an oxygen (O_2) gas phase—at technically relevant temperature and pressure will interact with the surfaces of metals and metal oxides. This implies that the material changes significantly; metals corrode (i.e., their surfaces become covered by metal oxides), and metal oxides assume a composition and structure at the surface that can be very different from what is known from ultrahigh-vacuum surface science studies. These oxides may be restricted to a thin film at the surface because of slow kinetics, but surface oxides may exist already as thermodynamically stable phases at conditions where the bulk oxide is not yet stable. This has recently been shown by DFT calculations.[4,5]

Surface oxide formation also plays a role under the conditions of catalysis when, in addition to O_2, reducing agents (e.g., carbon monoxide) are also present.[6] However, then the surface may be more or less far from thermodynamic equilibrium. Obviously, the chemical and physical properties of oxides (or surface oxides) are very different than those of metals, and whether they are stable or in a (frustrated) metastable configuration, they will affect the catalysis. Although this section uses oxidation catalysis as an example, analogies are expected for other situations (e.g., the formation of surface nitrides or hydrides).

One main example, ruthenium (the stable bulk oxide is RuO_2) is used here to address the basic concepts of *ab initio* atomistic thermodynamics, constrained thermodynamics, the stability of bulk and surface oxides, and *ab initio* statistical mechanics of adsorption and reaction dynamics to surfaces. Generalization to other late transition metals is briefly addressed as well. Only the basic theory is provided here; for details, see Reference 7 and the references therein.

Ab Initio *Atomistic Thermodynamics*

Although catalysis is not a thermodynamic equilibrium situation, knowledge of thermodynamic phases that may exist at or close to temperature and pressure (T, p) conditions of optimum catalyst

performance is important for any deeper analysis. When a material is in contact with a one-component gas or liquid phase, the environment can be described in terms of a reservoir uniquely characterized by its chemical potential. For an O_2 gas environment, used here as the example, we have

$$\mu_O(T, p) = 1/2[E_{O_2}{}^{\text{total}} + \mu_{O_2}(T, p^0) + 1/kT \ln (p/p^0)]. \quad (1)$$

This is the ideal gas equation, where the internal degrees of freedom of the O_2 molecule (vibrations and rotations) are contained in the $\mu_{O_2}(T, p^0)$ chemical potential term, as is the ideal gas entropy at the reference pressure $p^0 = 1$ atm. The $\mu_{O_2}(T, p^0)$ term and $E_{O_2}{}^{\text{total}}$, the total energy of the isolated molecule, can be computed by DFT. For details, see Reference 7.

A surface that is in contact with such a reservoir attempts to assume the lowest free energy by adsorbing oxygen or by transforming into an oxide. Alternatively, the system may transfer oxygen from the surface into the gas phase. Thus, plots of the free energies (calculated by DFT) of all plausible structures and stoichiometries as a function of $\mu_O(T, p)$ reveal the thermodynamically stable phases. Obviously, μ_O can be easily translated into a pressure (or ln p) axis for any given T or into a T axis for any given p.[7] Because the approach merges first-principles calculations of the atomic (and electronic) structure with concepts of thermodynamics, it was termed *ab initio* atomistic thermodynamics. It has been used to study defects in semiconductors and semiconductor surfaces and interfaces for a long time,[8,9] and since 1998[10] it has been widely employed to identify and analyze stable and metastable thermodynamic phases at metal and oxide surfaces.

Constrained Thermodynamics

For situations where the environment contains more than one component (e.g., O_2 as well as CO), the *ab initio* atomistic thermodynamics approach has been generalized.[11,12] Obviously, a full thermodynamic description is useless, as then O_2 and CO would not coexist but would form carbon dioxide (CO_2) with a significant energy gain (about 3 eV per CO_2 molecule). It is well known that this reaction does not happen on sensible time scales, because it is hindered by a significant free-energy barrier. Thus, it has been suggested to ignore CO_2 formation in a first theoretical attempt and consider two separate, independent reservoirs for O_2 and CO. Whereas the components are therefore not in equilibrium with each other, they are individually assumed to be in equilibrium with the surface.[11,12]

What is the value of such an approach? The lower regions of Figure 1, from the $O^{br}/-$ structure (bottom left, dark gray) to the O^{br}/O^{cus} structure (bottom right, black), reflect thermodynamically stable phases that exist when the CO concentration is negligible (the superscripts "br" and "cus"refer to the two important adsorption sites that exist on the surface, the "bridge" site and the "coordinatively unsaturated site," respectively). However, the light-gray region (O^{br}/CO^{cus}) does not represent a stable phase, because adsorbed O^{br} and adsorbed CO^{cus} will react to form CO_2. As O_2 has been dissociated already at the surface, the reactions will happen at a higher rate than *in vacuo*. A particularly interesting region is that between constrained phases. Here, not only O^{br} and CO^{cus} but also O^{cus} and CO^{cus} may react, and because pronounced fluctuations are to be expected, other reactions, namely, CO_2 formation via $O^{br} + CO^{br}$ and $O^{cus} + CO^{cus}$, may also become possible. What really happens at such border regions requires a careful analysis of the statistical mechanics, which is addressed later in the section on "*Ab Initio* Statistical Mechanics."

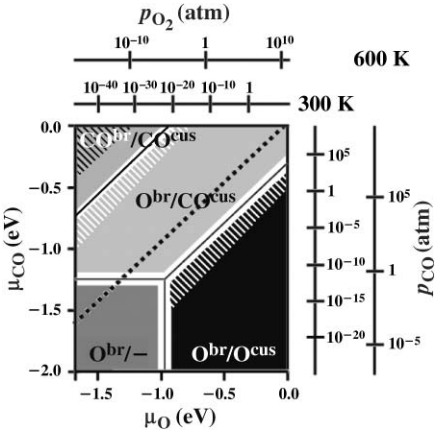

Figure 1. The atomic terminations of RuO_2(110) as obtained by constrained ab initio *atomistic thermodynamics. The superscripts "br" and "cus" refer to the two important adsorption sites that exist on the surface, the "bridge" site and the "coordinatively unsaturated site," respectively. Each can be occupied by O or by CO. In the upper-left region, above the black dotted line, bulk RuO_2 is not stable but will reduce to the Ru metal. The left and bottom axes note the chemical potentials, and the top and right axes provide two examples (T = 300 K and T = 600 K) for the corresponding pressures.*

Stability of Bulk and Surface Oxides

At the end of the 1990s, it became clear that the high catalytic activity of the Ru catalyst cannot be understood in terms of dissociation, adsorption, and reactions on the (pristine) Ru metal, but that the oxygen content in the surface region is significant.[4–6] When the Ru catalyst is in its highly active state, the surface is covered by RuO_2. In retrospect, this result is not surprising, because under the (T, p) conditions of catalysis, the Ru bulk oxide is in fact the stable phase.[13] As an example for other transition metals (from Ru to Ag), Figure 2 shows the results for the O-Ag(111) system.[4,5,14] Whereas silver oxide was considered previously to be unstable under catalytic conditions ($T \approx 450$ K), this theoretical work demonstrated that although bulk oxides cannot be formed, surface oxides may be present and active. In fact, for Ag(111), DFT calculations predict a variety of different surface oxides with nearly degenerate energies.[15] For other transition metals, the situation is analogous: when the transition metals are in contact with an O_2 atmosphere, they may develop thin surface oxides.[4,5,15] Experimental studies for rhodium (Rh) and palladium (Pd) confirmed these findings but also showed that the formation of surface oxides is slow, and under the experimental (surface science) conditions, thermodynamic equilibrium could not always be reached (see Reference 16 and references therein).

Reuter and Scheffler[13] studied the stability of the bulk oxides M_xO_y (with M = Ru, Rh, Pd, and Ag) under situations where

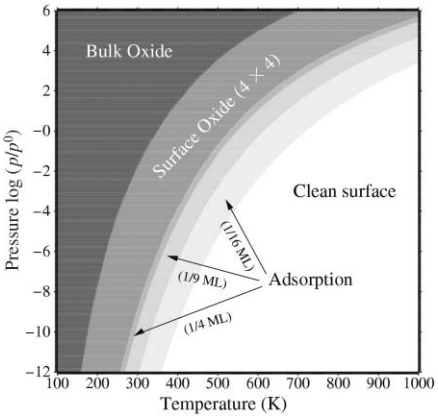

*Figure 2. Calculated (*T, p*) phase diagram for the O-Ag(111) system, showing the stable structures. Note that at conditions of catalysis, i.e., T ≈ 450 K and log(p/p⁰) ≈ 0, the bulk silver oxide is not stable. However, surface oxides of various stoichiometry may develop. ML stands for monolayer and 4 ×4 denotes the periodicity.*

not just O_2 but also the strongly reducing CO is present in the gas phase. Obviously, at high CO pressure, oxides are reduced to the clean metal. Under catalytic conditions, bulk Ru oxide was still found to be stable, but this is not the case for the other transition metals. Minute concentrations of CO may be sufficient to prevent the formation of bulk oxides for these systems.[13] Still, even in the presence of CO, surface oxides are close to forming, and this indeterminate state may be important for the catalytic function.

Ab Initio *Statistical Mechanics*

First-principles statistical mechanics starts with elaborate electronic-structure calculations to analyze all possibly relevant molecular processes, such as adsorption, desorption, diffusion of reactants, and surface chemical reactions. So far, our knowledge about these processes is still shallow, and a careful study, employing *ab initio* molecular dynamics (MD), is mandatory. *Ab initio* MD evaluates the forces on all the atoms using DFT and then feeds them into Newton's equation of motion to evaluate the dynamics of the atoms. In principle, that is all that is needed if the relevant time and length scales are covered. However, this is not the case: with *ab initio* MD, at most about 10 ps can be modeled, even on the most powerful supercomputer. For analyzing the function of materials, time spans that are 9–12 orders of magnitude longer are needed. Corrosion, for example, typically proceeds at a speed of about 1 atomic layer per minute.

To overcome these limitations, a systematic coarse-graining has been developed. The *ab initio* MD information is compressed into probabilities at which the various processes happen, and then the statistical mechanics of the many-atoms dynamics is solved using an extended kinetic Monte Carlo (kMC) approach (see Reference 17 and references therein). In simple words, this may be called "coarse-grained MD," and when done properly, no significant information is lost. An important aspect of an extended kMC scheme, considering well-defined atomistic processes, is that it also enables so-called reverse-mapping. Thus, the *ab initio* extended kMC scheme enables access to time scales of the order of seconds or longer, even for mesoscopically sized systems, while retaining the full atomistic information. It is then possible to identify which aspects of the electronic structure and which atomistic processes are actuating the catalytic function. For details of the method and its approximations, see References 7 and 17.

Studies of this kind have been employed to compute the composition, structure, and activity of the catalyst surface in reactive environments ranging from ultrahigh vacuum to technologically relevant conditions (see References 7 and 17 and references therein). These studies also provide a visualization of what happens under catalytic conditions at the atomic scale. Several aspects of these statistical mechanics results for the steady state of catalysis were surprising. For example, while under thermodynamic conditions all bridge sites of the $RuO_2(110)$ surface are occupied by oxygen atoms (the number of vacancies is far less than 1%), at the steady state of catalysis, the O^{br} occupation is only 90%. Note that the "steady state" is not a thermodynamic equilibrium. It refers to a thermodynamic open system and the steady production of CO_2 from incoming CO and O_2 molecules.

Another interesting point is that an unexpected short-range order builds up and suppresses reaction channels that, when just looking at energy barriers, would be assumed to be the most important.[17] The highest reactivity by far is found at the phase boundary (see the previous discussion of Figure 1), and the obtained value for the turnover frequency (CO_2 production) of 10^{18} cm^{-2} s^{-1} is in agreement with experimental work by Peden and Goodman.[18]

Understanding Trends in Reactivity

There are now a few reactions that are understood in some detail.[17,19] Such combinations of DFT calculations and kinetics are extremely demanding, and there is a strong need to develop concepts that assist in understanding trends in reactivity from one metal to the next without going into all the details. DFT calculations are also extremely important in this respect, and some simple models by which we are beginning to understand the overall trends are discussed here.

Grossly speaking, a surface reaction takes place in two overall steps. First, the reactants adsorb on the surface, typically by dissociating. If we take ammonia synthesis ($N_2 + 3H_2 \rightarrow 2NH_3$) over a transition-metal surface as the example, both N_2 and H_2 need to dissociate. The second step is the reaction of the surface species to form the product molecules. In the case of ammonia synthesis, these are the steps where adsorbed nitrogen is successively hydrogenated to form NH_3, which desorbs into the gas phase. A good catalyst must facilitate both the activation of the reactants and the formation of the products. The activation rate of the reactants will be given by the energy barrier for dissociation, E_a, and the formation rate of the products will be given by the adsorption energy, ΔE, of the atomically adsorbed intermediates on the surface. The stronger the adsorbate–surface bond (the more negative ΔE is), the higher the energy barrier for formation of the product will be. A good catalyst should have a small E_a and a small numerical value of ΔE. Unfortunately, calculations have shown that the two are strongly correlated for a number of molecules[20,21] (see Figure 3). A small barrier is therefore typically associated with a strong adsorbate–surface bond.

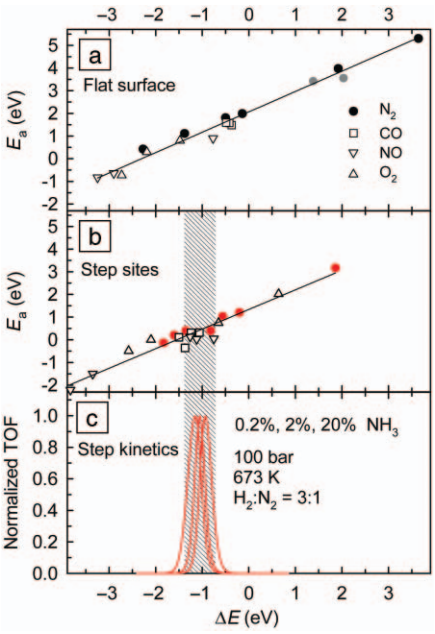

Figure 3. Calculated activation energies (transition-state potential energies) for N_2, CO, NO, and O_2 dissociation on a number of different metals, plotted as a function of the calculated dissociative chemisorption potential energy for the dissociation products. Results for (a) close-packed (flat) surfaces and (b) steps, showing the same trends but grouping along two different straight lines. The steps are more reactive than the terraces for these reactions. The linear relationship for N_2 dissociation on the most reactive step sites [red points in (b)] has been used as input into a kinetic model for the ammonia synthesis reaction. (c) The calculated reactivity per site per second (the turnover frequency, TOF), normalized to give the same maximum value, is shown for three different reaction conditions (red Gaussian peaks). (From Reference 20.) The vertical bar in (b) and (c) indicates the range of near-optimal dissociative chemisorption energies.

The reason for the linear correlation between the dissociation barrier and the adsorption energy is found by studying the nature of the transition states. Typically, they correspond to quite stretched molecules (see Figure 4), making the transition states seem as final-state, hence the correlation between the transition- and final-state energies.

The linear Brønsted–Evans–Polanyi (BEP)-type relationships between E_a and ΔE mean that the best catalyst must be a compromise with an intermediate value of the adsorption energy. This is a manifestation of the so-called Sabatier principle.[22] It is illustrated further in Figure 3, where the rate of reaction for ammonia synthesis is plotted as a function of ΔE, assuming the linear relationship with E_a. The "volcano" shape of the rate indicates that the optimum catalyst has a particular bond strength to the dissociated reactants. The fact that calculations can give a consistent set of activation energies and adsorption energies has paved the way for a semiquantitative analysis of the optimum bond strength for a given reaction.

Since different diatomic molecules have the same BEP relation, they would be expected to obey roughly the same general dependence of the reaction rate on the interaction strength. If ammonia kinetics is taken as a guideline, the optimum catalyst should be one with an adsorbate binding energy in the range of –1.1 ± 0.3 eV (Figure 3c). For ammonia synthesis (N_2 activation), both Ru and Fe lie within this range. For CO activation (Fischer–Tropsch synthesis), the same is true for Rh, Co, Ni, and Ru, and for NO activation it is Pd and Pt. For O_2 activation, none of the metals we considered are in the optimum range, but the closest are Ag (–0.65 eV), Pd (–1.56 eV), and Pt (–2.2 eV).[20] In all cases, these are metals known as some of the best catalysts for these reactions. The principle of an optimum adsorption energy is therefore in excellent agreement with experimental observations, suggesting that the BEP relationships are the core ingredient in rationalizing a large number of empirical data. It should be noted that the concepts of BEP relations, "volcanos," and the Sabatier principle are not restricted to metal surfaces. The same general principles apply to oxides, sulfides, nitrides, and carbides.

According to Figure 3, it is the variations in the dissociative adsorption energy of the reactants that control the trends in catalytic activity from one transition metal to the next. The calculations also enable an analysis of the electronic factors controlling these variations. Figure 5 shows how one particular property of the surface electronic structure, the average energy of the transition-metal *d*-states relative to the Fermi level, is largely responsible. The value of the *d*-band center projected onto the surface atoms involved in bonding turns out to not only explain variations in the adsorption energy from one metal to the next but also the effect of steps and other defects, strain, alloying, and adsorbate–adsorbate interactions.[24–29]

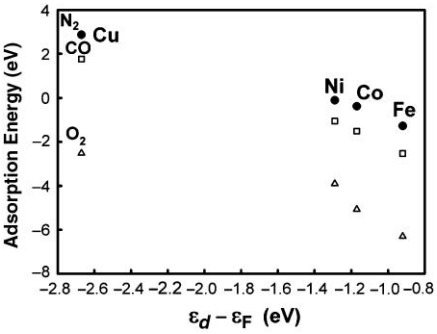

*Figure 5. Calculated dissociative N_2, CO, and O_2 chemisorption energies over different 3*d *transition metals plotted as a function of the center of the transition-metal* d*-bands. The term ε_d is the energy of the center of the* d*-band, while ε_F is the Fermi-level energy. (From Reference 23.) Filled circles represent N_2, open squares CO, and open triangles O_2.*

Applications in Industry: Improved Catalysts for Producing Ultralow-Sulfur Fuels

As mentioned in the Introduction, large sectors of industry are dependent on heterogeneous catalysis. This section illustrates how insight provided by DFT calculations has already been used in the development of new catalysts in industry by concentrating on the catalytic processes employed to remove sulfur-containing molecules from fossil fuels. The societal demand for ultraclean fuels, with a maximum of 50 ppm sulfur currently, required catalyst manufacturers to double the activity per unit volume of hydrodesulfurization (HDS) catalysts in less than 10 years.[30] This has been possible through a tremendous research effort, to which DFT contributed much.

Industrial HDS catalysts in their active state may be described as nanoparticles of ternary transition-metal sulfides (TMSs) associating Co or Ni to Mo or W, supported over nanoparticles of cubic γ-alumina. The active nanoparticles look like the image in Figure 6, which is a roughly hexagonal patch cut off a single layer of MoS_2 (WS_2 is isostructural). The basal planes are capped by tri-coordinated S and inert. Active sites are on the edges, where undercoordinated metal ions appear. The promoter atoms, Co or Ni, substitute Mo or W at the edges. Early ideas of this particular self-organization[31,32] were recently supported by detailed DFT investigations[33,34] that showed the substitutional position to be energetically favored and led to the best match of local structures with available experimental data (e.g., Co-S, Mo-S, and Co-Mo distances and numbers of average first-and second-neighbors from extended x-ray absorption fine structure). Scanning tunneling microscopy (STM) studies of gold-supported preparations of such

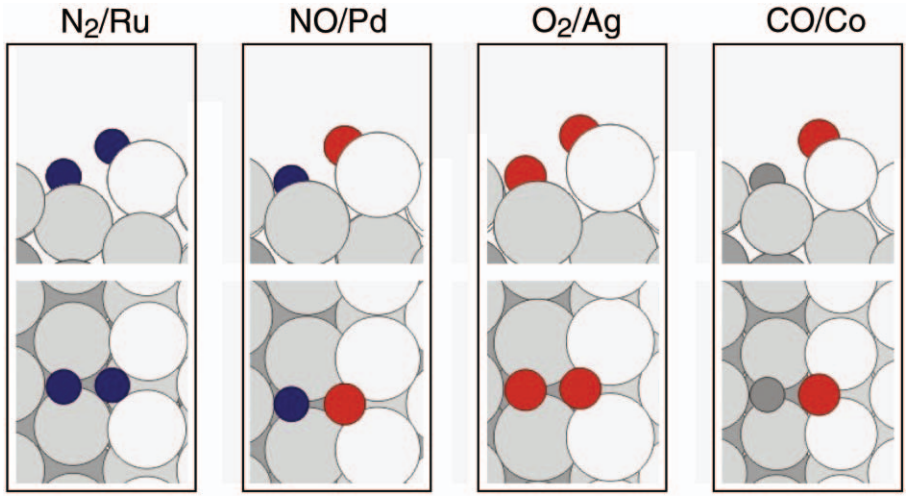

Figure 4. Calculated transition-state structures for N_2, NO, O_2, and CO dissociation on different transition-metal surfaces. Results for close-packed surfaces are shown in the upper row and for stepped surfaces in the lower row. N is shown in blue, O in red, and C in gray. (From Reference 20.)

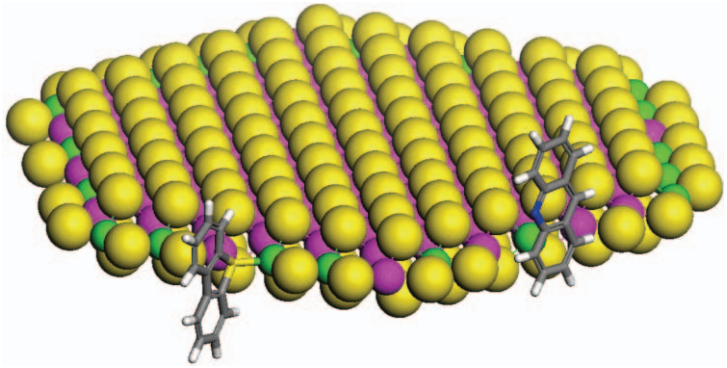

Figure 6. Model in perspective view of an active CoMoS nanoparticle in interaction with dibenzothiophene on a S-edge and acridine on a Mo-edge. (H, white; C, gray; S, yellow; N, blue; Co, green; and Mo, pink). (Courtesy of P. Raybaud, Institut Français du Pétrole.)

particles[35,36] provided magnificent direct observations of these structures. DFT calculations provided the necessary clues for a precise interpretation of images[37,38] in terms of the underlying geometrical and electronic structures, and through *ab initio* atomistic thermodynamics (as described earlier), they also provide the link between the observations under ultrahigh-vacuum conditions and the active state of the catalyst under reaction conditions.

The influence of the gas-phase (H_2+ H_2S) composition and temperature on the equilibrium shape of the nanoparticles has been among the most remarkable of the insights brought by DFT and confirmed by STM. Making use of *ab initio* atomistic thermodynamics,[7] all surface energies were evaluated by DFT as functions of controlling chemical potentials, so that surface phase diagrams and morphology diagrams could be constructed. Basal (0001) planes have negligible surface energies, compared with the two crystallographically unequivalent S-edge and $(\bar{1}010)$ Mo-edge $(10\bar{1}0)$ planes. At usual operating conditions for HDS processes, the surface tensions for the two edges are comparable, and morphologies are thus approximately hexagonal. Subtle differences remain, however, between the CoMoS and NiMoS systems;[39] for instance, at HDS conditions, Co prefers to sit at S-edges, whereas Ni decorates both edges. Major steps have thus been achieved toward an atomistic description of active sites *in operando* for these important systems.

Important new insight into the active site for HDS was obtained by the combined DFT and STM discovery that around the edge of the nanoparticles, the otherwise insulating MoS_2 becomes metallic[35,36,40] and that these metallic "brims" are important for the catalytic chemistry.[41]

The precise nature of the interaction of the TMS active nanoparticles with γ-alumina nanoparticles is a very challenging question. The formerly controversial γ-Al_2O_3 structure is produced by controlled topotactic dehydration of ultrafine (e.g., nanoparticular) boehmite (AlOOH), a layered mineral.[42] It was possible to find a reasonable pathway for this solid–solid reaction, along which the free-energy profile was evaluated by DFT.[43] A model bulk structure resulted, the computed properties of which match nicely the known characteristics of γ-Al_2O_3.[44] Again, using *ab initio* atomistic thermodynamics, the nature and density of the various hydroxyl groups terminating the low Miller index surfaces dominating the morphology inherited from boehmite were described according to experimental conditions.[45] O–H bond-stretching vibration frequencies were determined on the basis of the DFT potential energy surfaces and compared to the experimental Fourier transform infrared spectra of γ-Al_2O_3 available as a function of pretreatment conditions. A striking agreement allowed a complete reassignment of these spectra in terms of precise local coordination of hydroxyls and the particular facets involved. A detailed analysis of Lewis and Brønsted acid–basic properties of γ-Al_2O_3 surfaces was also provided.[44] Determining the stable surface terminations in the presence of both water and H_2S[46] was a prerequisite for the direct DFT simulation of (smaller) MoS_2 aggregates interacting with the different alumina surfaces, so as to determine the stable configurations *in operando*.[47] Similar studies are ongoing for the promoted systems, revealing generally weaker interactions under the same conditions (Figure 7).[48]

Experimental activities of binary TMS[49] follow nicely a "volcano" curve when plotted against a DFT-computed estimate of the metal–sulfur bond strength E_{MS} within the bulk material (Figure 8).[50,51] This is another illustration of the Sabatier principle, analogous to that shown in Figure 3; therefore, this principle explains the synergetic effect in ternaries used industrially. E_{MS} should then provide a relevant descriptor when more complex TMS structures are screened for potentially HDS-active materials. In such a search

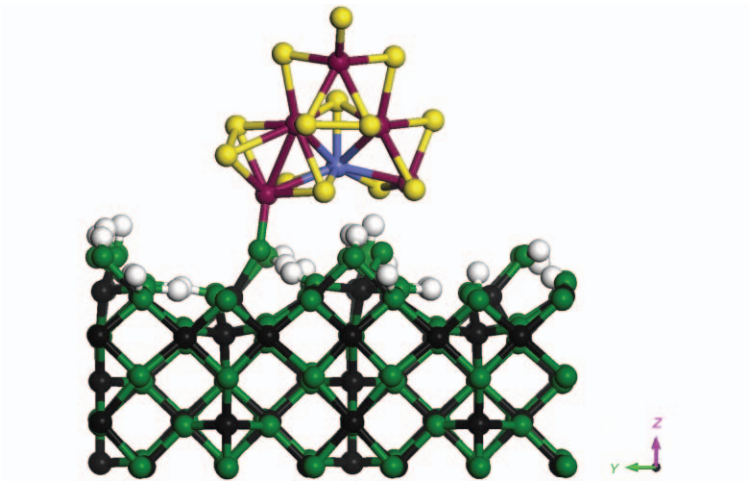

Figure 7. DFT-optimized model of minimal CoMoS aggregate in interaction with the (110) surface of γ-Al_2O_3 under hydrodesulfurization conditions. It is predicted that one strong iono-covalent Mo–O bond binds the active aggregate to the support, while the promoter Co atom remains in the same coordination as in the standalone aggregate. (H, white; O, green; Al, black; S, yellow; Co, blue; and Mo, red). (Courtesy of D. Costa, Institut Français du Pétrole.)

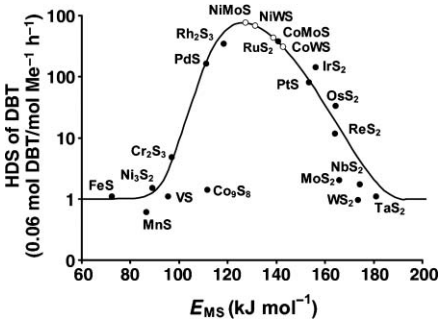

Figure 8. The Sabatier principle applied to the catalysis of hydrodesulfurization (HDS) by transition-metal sulfides. Solid dots: experimental catalytic activity data for HDS of dibenzothiophene (DBT) from Reference 49 in ordinates, and DFT-calculated metal–sulfur bond energies in abscissa. Open dots: predicted activities for mixed sulfides in ordinates, DFT-calculated strength of the metal–sulfur bond, E_{MS}, in abscissa. The solid curve is a prediction of a microkinetic model. (Adapted from References 50 and 51.)

through structural databases[52] recently undertaken at the Institut Français du Pétrole, dozens of structures were rapidly examined, some of them quite complex with large unit cells, among which 20% turned out to have E_{MS} falling in the interval of interest. Among these hits, Cr_2NiS_4 was simultaneously and independently reported active.[53] Other promising and original structures are under experimental investigation. Many challenges are ahead in order to compete with the highly optimized Co(Ni)Mo(W)S/γ-Al_2O_3 state-of-the-art systems.

Conclusions

We have tried to illustrate how density functional theory calculations are helping to develop a detailed molecular-level picture of heterogeneous catalysis. We are beginning to get a better understanding of the state of the active catalyst, the mechanism and kinetics, and the trends in reactivity for classes of reactions and catalysts. DFT has brought new insight that has already played a significant part in the design of new preparation methods in industry. Moreover, DFT opens exciting prospects for the discovery of new catalysts, a learned alternative to blind search.

There is a long way to go before we have a general theoretical description of heterogeneous catalysis. Catalysts are complicated, multiphase materials, and there are an enormous number of interesting catalytic processes. We are just at the beginning of an era where DFT calculations contribute a new perspective to the many important experimental tools that have been developed to understand surface reactivity.

References

1. I. Maxwell, *Stud. Surf. Sci. Catal.* **101** (1996) p. 1.
2. F. Haber, Nobel Prize Lecture (1919); C. Bosch, Nobel Prize Lecture (1932).
3. P. Cong, R.D. Doolen, Q. Fan, D.M. Giaquinta, S. Guan, E.W. McFarland, D.M. Poojary, K. Self, H.W. Turner, and W.H. Weinberg, *Angew. Chem. Int. Ed.* **38** (1999) p. 484.
4. W.-X. Li, C. Stampfl, and M. Scheffler, *Phys. Rev. Lett.* **90** 256102 (2003).
5. W.-X. Li, C. Stampfl, and M. Scheffler, *Phys. Rev. B* **67** 045408 (2003).
6. C. Stampfl, M.V. Ganduglia-Pirovano, K. Reuter, and M. Scheffler, *Surf. Sci.* **500** (2002) p. 368.
7. K. Reuter, C. Stampfl, and M. Scheffler, *Handbook of Materials Modeling*, Vol. 1, edited by S. Yip (Springer, Berlin, 2005) p. 149.
8. C.M. Weinert and M. Scheffler, in *Defects in Semiconductors*, edited by H.J. von Bardeleben, *Mat. Sci. Forum* **10–12** (1986) p. 25.
9. M. Scheffler and J. Dabrowski, *Phil. Mag. A* **58** (1988) p. 107.
10. X.-G. Wang, W. Weiss, Sh.K. Shaikhutdinov, M. Ritter, M. Petersen, F. Wagner, R. Schlögl, and M. Scheffler, *Phys. Rev. Lett.* **81** (1998) p. 1038.
11. K. Reuter and M. Scheffler, *Phys. Rev. Lett.* **90** 046103 (2003).
12. K. Reuter and M. Scheffler, *Phys. Rev. B* **68** 045407 (2003).
13. K. Reuter and M. Scheffler, *Appl. Phys. A* **78** (2004) p. 793.
14. A. Michaelides, M.-L. Bocquet, P. Sautet, A. Alavi, and D.A. King, *Chem. Phys. Lett.* **367** (2003) p. 344.
15. A. Michaelides, K. Reuter, and M. Scheffler, *J. Vac. Sci. Technol. A* **23** (2005) p. 1487.
16. G. Ketteler, D.F. Ogletree, H. Bluhm, H. Liu, E.L.D. Hebenstreit, and M. Salmeron, *J. Am. Chem. Soc.* **127** (2005) p. 18269.
17. K. Reuter, D. Frenkel, and M. Scheffler, *Phys. Rev. Lett.* **93** 116105 (2004); *Phys. Rev. B* **73** 045433 (2006).
18. C.H.F. Peden, D.W. Goodman, D.S. Blair, P.J. Berlowitz, G.B. Fisher, and S.H. Oh, *J. Phys. Chem.* **92** (1988) p. 1563.
19. K . Honkala, A. Hellman, I.N. Remediakis, A. Logadottir, A. Carlsson, S. Dahl, C.H. Christensen, and J.K. Nørskov, *Science* **307** (2005) p. 555.
20. J.K. Nørskov, T. Bligaard, A. Logadottir, S. Bahn, L.B. Hansen, M. Bollinger, H. Bengaard, B. Hammer, Z. Sljivancanin, M. Mavrikakis, Y. Xu, S. Dahl, and C.J.H. Jacobsen, *J. Catal.* **209** (2002) p. 275.
21. A. Michaelides, Z.-P. Liu, C.P. Zhang, A. Alavi, D.A. King, and P. Hu, *J. Am. Chem. Soc.* **125** (2003) p. 3704.
22. P. Sabatier, *La catalyse en chimie organique* (Bérange, Paris, 1920).
23. A. Nilsson, L.G.M. Pettersson, B. Hammer, T. Bligaard, C.H. Christensen, and J.K. Nørskov, *Catal. Lett.* **100** (2005) p. 111.
24. B. Hammer and J.K. Nørskov, *Nature* **376** (1995) p. 238.
25. M. Mavrikakis, B. Hammer, and J.K. Nørskov, *Phys. Rev. Lett.* **81** (1998) p. 2819.
26. V. Pallassana and M. Neurock, *J. Catal.* **191** (2000) p. 301.
27. O.M. Lovvik, R.A. Olsen, *J. Chem. Phys.* **118** (2003) p. 3268.
28. A. Roudgar and A. Gross, *Phys. Rev. B* **67** 033409 (2003).
29. M. Gajdos, A. Eichler, and J. Hafner, *J. Phys.: Cond. Matt.* **16** (2004) p. 1141.
30. See Axens IFP Group Technologies Web site, www.axens.fr, and Haldor Topsoe Web site, www.topsoe.com (accessed August 2006).
31. H. Topsoe, B.S. Clausen, R. Candia, C. Wivel, and S. Morup, *J. Catal.* **68** (1981) p. 433.
32. S. Kasztelan, H. Toulhoat, J. Grimblot, and J.P. Bonnelle, *Appl. Catal.* **13** (1984) p. 127.
33. L. Byskov, J.K. Nørskov, B.S. Clausen, and H. Topsøe, *J. Catal.* **187** (1999) p. 109.
34. P. Raybaud, J. Hafner, G. Kresse, S. Kasztelan, and H. Toulhoat, *J. Catal.* **190** (2000) p. 128.
35. S. Helveg, J.V. Lauritsen, E. Lægsgaard, I. Stensgaard, B.S. Clausen, H. Topsøe, and F. Besenbacher, *Phys. Rev. Lett.* **84** (2000) p. 951.
36. J.V. Lauritsen, S. Helveg, E. Laegsgaard, I. Stensgaard, B.S. Clausen, H. Topsøe, and F. Besenbacher, *J. Catal.* **197** (2001) p. 1.
37. H. Schweiger, P. Raybaud, G. Kresse, and H. Toulhoat, *J. Catal.* **207** (2002) p. 76.
38. M.V. Bollinger, K.W. Jacobsen, and J.K. Nørskov, *Phys. Rev. B* **67** 085410 (2003).
39. H. Schweiger, P. Raybaud, and H. Toulhoat, *J. Catal.* **212** (2002) p. 33.
40. M.V. Bollinger, J.V. Lauritsen, K.W. Jacobsen, J.K. Nørskov, S. Helveg, and F. Besenbacher, *Phys. Rev. Lett.* **87** 196803 (2001).
41. J.V. Lauritsen, M. Nyberg, R.T. Vang, M.V. Bollinger, B.S. Clausen, H. Topsøe, K.W. Jacobsen, J.K. Nørskov, and F. Besenbacher, *Nanotechnology* **14** (2003) p. 385.
42. P. Euzen, P. Raybaud, X. Krokidis, H. Toulhoat, J.L. Le Loarer, J.P. Jolivet, and C. Froidefond, in *Handbook of Porous Materials*, Ch. 4, 7, and 9, edited by F. Schüth, K. Sing, and J. Weitkamp (Wiley VCH, Weinheim, 2002) p. 1591.
43. X. Krokidis, P. Raybaud, A.E. Gobichon, B. Rebours, P. Euzen, and H. Toulhoat, *J. Phys. Chem. B* **105** (2001) p. 5121.
44. M. Digne, P. Sautet, P. Raybaud, P. Euzen, and H. Toulhoat, *J. Catal.* **226** (2004) p. 54.
45. M. Digne, P. Sautet, P. Raybaud, P. Euzen, and H. Toulhoat, *J. Catal.* **211** (2002) p. 1.
46. C. Arrouvel, M. Breysse, H. Toulhoat, and P. Raybaud, *J. Catal.* **226** (2004) p. 260.
47. C. Arrouvel, M. Breysse, H. Toulhoat, and P. Raybaud, *J. Catal.* **232** (2005) p. 161.
48. D. Costa, H. Toulhoat, and P. Raybaud, unpublished.
49. T.A. Pecoraro and R.R. Chianelli, *J. Catal.* **67** (1981) p. 430.
50. H. Toulhoat, P. Raybaud, S. Kasztelan, G. Kresse, and J. Hafner, *Catal. Today* **50** (1999) p. 629.
51. H. Toulhoat and P. Raybaud, *J. Catal.* **216** (2003) p. 63.
52. Materials Design Web site, www.materialsdesign.com (accessed August 2006).
53. A. Thiollier, P. Afanasiev, P. Delichere, and M. Vrinat, *J. Catal.* **197** (2001) p. 58. □